Antibody–Drug Conjugate Sacituzumab Govitecan Drives Efficient Tissue Penetration and Rapid Intracellular Drug Release

Anna Kopp[1], Scott Hofsess[2], Thomas M. Cardillo[2], Serengulam V. Govindan[2], Jennifer Donnell[2], and Greg M. Thurber[1,3,4]

ABSTRACT

Antibody–drug conjugates (ADC) are a rapidly growing class of targeted cancer treatments, but the field has experienced significant challenges from their complex design. This study examined the multiscale distribution of sacituzumab govitecan (SG; Trodelvy), a recently clinically approved ADC, to clarify the mechanism(s) of efficacy given its unique design strategy. We employed a multiscale quantitative pharmacokinetic approach, including near-infrared fluorescence imaging, single-cell flow cytometry measurements, payload distribution via γH2AX pharmacodynamic staining, and a novel dual-labeled fluorescent technique to track the ADC and payload in a high trophoblast cell-surface antigen 2 expression xenograft model of gastric cancer (NCI-N87). We found that rapid release of the SN-38 payload from the hydrolysable linker inside cells imparts more DNA damage *in vitro* and *in vivo* than an ADC with a more stable enzyme cleavable linker. With SG, little to no extracellular payload release in the tumor was observed using a dual-labeled fluorescence technique, although bystander effects were detected. The high dosing regimen allowed the clinical dose to reach the majority of cancer cells, which has been linked to improved efficacy. In addition, the impact of multiple doses (day 1 and day 8) of a 21-day cycle was found to further improve tissue penetration despite not changing tumor uptake [percent injected dose per gram (%ID/g)] of the ADC. These results show increased ADC efficacy with SG can be attributed to efficient tumor penetration and intracellular linker cleavage after ADC internalization. This quantitative approach to study multiscale delivery can be used to inform the design of next-generation ADCs and prodrugs for other targets.

Introduction

Antibody–drug conjugates (ADC) form a class of targeted chemotherapy that combines the specific targeting of a monoclonal antibody with the cytotoxicity of a small molecule payload, attached via a chemical linker. Recent developments have resulted in a surge of seven FDA approvals in 3 years despite previous setbacks from other late-stage clinical failures. One of the recent approvals includes sacituzumab govitecan (SG), a novel ADC composed of an anti—trophoblast cell-surface antigen 2 (Trop-2) antibody coupled to the SN-38 payload via a proprietary, hydrolysable CL2A linker, targeting triple-negative breast cancer (TNBC) and urothelial cancer (UC). Trop-2 is a 45 kDa transmembrane glycoprotein, first recognized as a trophoblast cell-surface marker, and was later found to be expressed in epithelial cancers. It is a novel ADC target involved in a number of cell proliferating signaling pathways including cyclin D1, NF-κB, and ERK/MEK (1). Trop-2 is expressed in a wide range of cancers, including gastric, pancreatic, TNBC, UC, prostate, as well as lung cancer, and expression of Trop-2 correlates with increased tumorigenicity and poor prognosis in patients (2, 3). SN-38 (the active drug form of irinotecan) is a topoisomerase I inhibitor that causes DNA double-strand breaks during replication, leading to cell-cycle arrest (4). Treating solid tumors with ADCs versus hematologic cancers presents additional hurdles, which are partially explained by poor delivery and tumor penetration of ADCs (5). SG has several unique attributes including a high 10-mg/kg dosing regimen, a high drug to antibody ratio (DAR) of 7.6, a unique chemically hydrolysable CL2A linker, and the moderately potent SN-38 payload. However, the roles of these unique features in the success of SG remain unclear.

SG marks a shift in common ADC design approaches, many of which focus on using highly stable, conditionally cleavable linkers with ultrapotent payloads (i.e., pmol/L IC_{50} values; ref. 6). Notably, this lower payload potency enables SG to use the highest clinical dosing regimen of all FDA-approved ADCs: a 10-mg/kg dose administered on days 1 and 8 of a 21-day cycle. The efficacy of SG has been demonstrated both preclinically (7, 8) and clinically (9–11). However, the overall disposition of ADCs and their payloads are complex (**Fig. 1**), and several questions remain around the quantitative pharmacology of using moderately potent payloads with hydrolysable linkers, especially considering the diverging design strategy from previously approved ADCs.

Linker selection is important for ADC design because it influences the threshold for toxicity and efficacy by modulating payload release in circulation, off-target tissues, and cancer cells. Ideally, a linker would release the payload efficiently and specifically in cancer cells alone. However, payloads can be released in circulation or in healthy cells after target-mediated or nonspecific accumulation in other tissues, leading to toxicity and complex pharmacokinetics. Therefore, there has been a significant effort in the ADC field to engineer more stable linkers to minimize off-target toxicity (12, 13). Protease cleavable linkers are one of the most common linkers given their stability in circulation and ability to release payload upon cleavage inside cells. In contrast, SG uses a benzyl carbonate linker that can be hydrolyzed at neutral or acidic pH including in systemic circulation [half-life of

[1]Department of Chemical Engineering, University of Michigan, Ann Arbor, Michigan. [2]Gilead Sciences, Inc., Morris Plains, New Jersey. [3]Department of Biomedical Engineering, University of Michigan, Ann Arbor, Michigan. [4]Rogel Cancer Center, University of Michigan, Ann Arbor, Michigan.

Corresponding Author: Greg M. Thurber, University of Michigan, 2800 Plymouth Rd., Ann Arbor, MI 48109. Phone: 734-764-8722; E-mail: gthurber@umich.edu

Mol Cancer Ther 2023;22:102–11

doi: 10.1158/1535-7163.MCT-22-0375

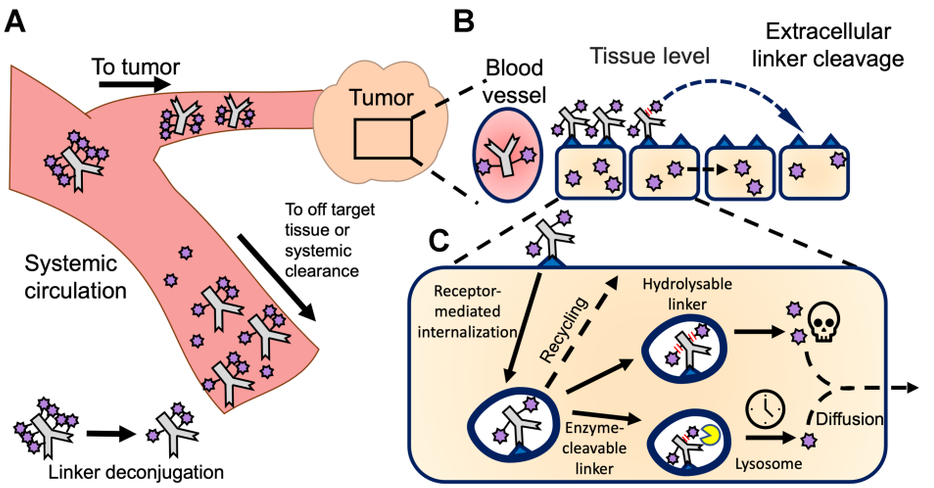

Figure 1.
Multiscale pharmacokinetics of ADCs. **A,** ADCs in systemic circulation distribute to both tumor and healthy tissue, where they can bind their target and release the payload. In addition, deconjugation in the systemic circulation releases payload, lowering the DAR. **B,** Within the tumor, ADCs extravasate, diffuse through the tissue, bind their target, internalize, and release the payload via hydrolysis or protease cleavage for CL2A and CL2E linkers, respectively. Linker hydrolysis can also occur extracellularly, and released payload can diffuse to nearby cells (bystander effect).

payload release in human serum = 20.3 hours (8); see also supplementary discussion].

Increased linker stability can prevent payload release in circulation and increase delivery to the tumor, because systemic release prevents targeted delivery to the tumor. However, previous results showed that the protease-cleavable linker (higher stability) was less effective than the hydrolysable linker (lower stability; refs. 14, 15). One potential benefit of the hydrolysable linker is less target-mediated toxicity. By avoiding sustained Trop-2–mediated delivery to healthy tissue, SG has avoided stomatitis and other target-mediated toxicity of previous Trop-2 ADCs (16). While it is logical that hydrolysis could lower target-mediated uptake in healthy tissue, it is not clear why the hydrolysable linker is more effective in the tumor, a focus of this work.

After internalization, ADCs are trafficked to lysosomes where antibody degradation and payload release occurs. A previous publication found efficient trafficking to the lysosomes can improve Trop-2 ADC efficacy (17). A hydrolysable linker could be cleaved during trafficking, bypassing the need for lysosomal delivery for payload release to improve efficacy. In addition, a significant fraction of linker could be cleaved outside the cell membrane, releasing SN-38 within the tumor microenvironment to mediate bystander killing. The bystander effect refers to the ability of payloads prior to or during internalization, to diffuse through membranes out of directly targeted cells into neighboring untargeted cells (18). SN-38 has been confirmed to exhibit bystander killing (19, 20), but the impact of bystander killing on efficacy is not fully understood, especially because it has been found to be less efficient than direct cell killing (21).

Two hypotheses were examined for improved ADC efficacy with the hydrolysable linker: (i) increased efficiency of intracellular release and/or (ii) increased extracellular release and bystander killing. To test these hypotheses, we quantified the multiscale distribution of SG to elucidate the quantitative pharmacology of the hydrolysable linker, high dosing regimen, and moderately potent payload of SG. Three ADCs were used: (i) SG, hRS7-CL2A-SN-38, (ii) SG modified with a more stable enzyme-cleavable linker, hRS7-CL2E-SN-38, and (iii) a nonspecific negative control antibody with the same hydrolysable linker and payload as SG, h679-CL2A-SN-38. Structures and syntheses of linker-payloads, CL2A-SN-38 and CL2E-SN-38, have been described previously (8, 22). Using quantitative fluorescence techniques, the multiscale ADC distribution and payload efficacy (via γH2AX staining of DNA damage) were tracked *in vitro* and *in vivo* to determine how each linker influenced the intracellular payload release and the bystander effect. We also used a dual-labeled fluorescence technique to determine the location of linker release (intracellular vs. extracellular). The results of these analyses together demonstrate the multiscale distribution and efficacy of SG.

Materials and Methods

Cell culture and animals

The NCI-N87 cell line was purchased from ATCC and maintained according to ATCC recommendations. Cells were stored at 37°C in 5% CO_2 and passaged 2 to 3 times per week up to passage 50 using RPMI1640 (NCI-N87) each supplemented with 10% (v/v) FBS, 50 U/mL penicillin and 50 μg/mL streptomycin. *Mycoplasma* tests were performed annually using Mycoalert Testing Kit (Lonza). All animal studies were performed in accordance with and approval from the University of Michigan Institutional Animal Care and Use Committee and Association for Assessment and Accreditation of Laboratory Animal Care International guidelines in 6- to 8-week-old female nude mice (Jackson Labs). Briefly, 5 million NCI-N87 cells were injected subcutaneously into the left flank in 50% v/v Matrigel (Fisher Scientific) and treated as described below.

ADC and fluorescent antibody labeling with AlexaFluor680

SG (hRS7-CL2A-SN-38), enzyme-cleavable linker ADC (hRS7-CL2E-SN-38), and nonspecific antibody negative control ADC (h679-CL2A-SN-38) were prepared as previously described (8, 22). Conjugates were stored in lyophilized form at −20°C until reconstitution, after which CL2A conjugates were either discarded within one hour or flash frozen and stored at −80°C until future use. hRS7 antibody was conjugated to AlexaFluor680 (AF680, Fisher Scientific) for biodistribution, plasma clearance, and tumor digest experiments as previously described via NHS ester chemistry to obtain a final degree of labeling of approximately 0.3 to prevent changes in distribution upon conjugation of dye (23). For experiments involving dual fluorescent labels, the antibody was stably labeled with AlexaFluor488 (AF488, Fisher Scientific), while SN-38 component of CL2A-SN-38 was stably labeled with near IR dye, AF680, at the drug's 10-hydroxy position. CL2A-SN-38-AF680 was conjugated to reduced AF488-hRS7 by the standard thiol-maleimide chemistry (details provided in Supplemental Information).

In vitro pharmacodynamic staining with phospho-histone H2A.X

NCI-N87 cells were plated at 5×10^5 cells/well in a 24-well plate for flow cytometry or 1.5×10^5 cells/well in Falcon 8-well chamber slides for imaging and allowed to adhere overnight. Cells were then treated with 40 nmol/L SG, hRS7-CL2E-SN38, or h679-CL2A-SN38 (non-specific control) for an 8-hour pulse in complete media, then washed twice after the removal of ADC and was replaced with complete media without ADC for a 24-, 48-, or 72-hour chase phase. At the end of each chase, cells were washed twice with PBS, then 500-mL trypsin warmed to 37°C was added to each well to detach cells for flow cytometry. After cells were fully detached, they were washed once in PBS containing 0.5% BSA, then fixed using BD Cytofix Fixation buffer (BD Biosciences). Fixed cells were stored at 4°C until timepoints concluded. Cells were then permeabilized using 1X BD Cytoperm (BD Biosciences) buffer in PBS-BSA.

Cells were stained using the Phospho-Histone H2A.X (Ser139; 20E3) rabbit primary antibody (Cell Signaling Technology) as a marker for double stranded DNA breaks at 0.15 μg/mL in 0.5% BSA/Perm buffer for 30 minutes. Cells were washed twice with BSA/Perm buffer, then incubated for 30 minutes with a 1,200× dilution of secondary goat-anti-rabbit-Fab2 fragment labeled with AlexaFluor488 for flow cytometry experiments or AlexaFluor555 for imaging experiments (Cell Signaling Technology). After the 30-minute incubation, cells were washed twice in BSA/Perm buffer. Cells were kept in the dark and on ice for all incubations. Cells were then analyzed on an Attune NxT flow cytometer and data were analyzed using FlowJo software. Cell nuclei were stained with Hoechst 33342 (Invitrogen) for 1 minute before imaging, which was performed on the Olympus FV1200 confocal microscope using 405- and 543-nm lasers and a 60× objective. Images were analyzed using ImageJ software.

Plasma clearance with fluorescent hRS7

Following the tail vein injection of fluorescent hRS7 at a 5 mg/kg or 10 mg/kg dose, blood samples were collected into hematocrit tubes by retro-orbital blood sampling. Ten microliter of whole blood was mixed with 15 μL of 10 mmol/L PBS-EDTA to prevent clotting, then was centrifuged for 2,500 x *g* for 2 minutes. The plasma supernatant was removed and stored at −80°C until analysis. Samples were scanned on the NIR Odyssey CLx Scanner (LI-COR) in a 384-well black walled plate for samples in the NIR range. When dual-labeled hRS7 was used, 15-μL plasma was run on an SDS-PAGE gel, scanned on an Odyssey M scanner (LI-COR), and analyzed using ImageStudio software. The plasma concentration was normalized to initial concentration and fit to a biexponential decay in PRISM (GraphPad).

Biodistribution with fluorescent hRS7

Biodistribution was performed as previously described (24). Either 24 or 48 hours after tail vein injection with fluorescent hRS7, mice were euthanized and organs were then resected and mechanically disrupted. A solution of 5 mg/mL collagenase IV (Worthington Biochemical) in 1X RIPA cell lysis buffer (Fisher Scientific) was then added to the organs for a 1-hour incubation. Organs were sonicated using an FB-120 Sonic Dismembrator and incubated for another hour after adding 1X RIPA buffer with 0.025% trypsin-EDTA. Cells were sonicated again to complete tissue homogenization, then serially diluted and scanned on the Odyssey CLx Scanner. A calibration curve of known concentration was used to calculate the concentration of fluorescent probe, which was then normalized to organ weight and dose to calculate the %ID/g.

Single-cell tumor digests

Tumors were digested into single-cell suspensions using the Tumor Dissociation Kit (Miltenyi Biotech) according to the manufacturer's instructions, then resuspended in media containing 10% FBS to quench enzymes and filtered through a 40-μm filter to reduce clumping. Subsets of single cells were stained *ex vivo* with 40 nmol/L fluorescent hRS7 to determine percent of cells targeted. Cells were analyzed on an Attune NxT flow cytometer.

Histology with fluorescence microscopy

Fluorescence microscopy was used to analyze the antibody/ADC distribution in tumors after intravenous injections. Mice were injected with 15 mg/kg Hoechst 33342 15 minutes before sacrifice to label functional blood vessels. Tumors were resected, flash frozen in OCT, and stored at −80°C until cryostat sectioning into 12-μm slices. Tumors with fluorescent hRS7 were stained using anti-mouse CD31 (BioLegend) labeled with AlexaFluor555 for 30 minutes. Tumors that were treated with ADCs were stained with the previously stated pharmacodynamics (PD) staining procedure outlined above and an anti-human Fc antibody labeled with FITC (BioLegend). An Olympus FV1200 microscope was used for imaging with 405-, 488-, 543-, and 635-nm lasers with a 20× objective. Image analysis was performed using ImageJ software.

Data availability

The data generated in this study are available upon request from the corresponding author.

Results

In vivo hRS7 multiscale distribution studies

Mice bearing NCI-N87 tumors were dosed with either 5 mg/kg or 10 mg/kg (the clinical dose in mg/kg, see Supplemental Data for discussion) of fluorescent hRS7 to study dose-dependent tissue penetration, tumor uptake, and percent of single cells targeted (**Fig. 2**). The tissue penetration at the clinical dose, confirmed via fluorescent imaging of tumor sections (**Fig. 2A** and **B**), showed relatively homogeneous distribution after a single 10-mg/kg dose of hRS7. Organ level biodistribution measurements showed no significant difference in tumor antibody uptake at 24 or 48 hours (**Fig. 2C**). This was also consistent with quantitative, single-cell data collected from tumor digests analyzed on flow cytometry (**Fig. 2D**; Supplementary Fig. S1). On the basis of comparison with cells that are stained with fluorescent antibody *ex vivo*, it was determined that a majority of cells (68.8%) were targeted with hRS7 after a 10-mg/kg dose compared with 38.9% after a 5-mg/kg dose. Because tissue penetration scales with C_{max} and plasma concentrations are slightly higher in humans than mice at this dose, the results indicate efficient tissue penetration at these doses. Overall, the data are consistent with the high dosing of SG, enabled by the moderate potency payload, driving efficient tumor tissue penetration.

ADC PD staining *in vitro*

PD staining of γH2AX marks double-stranded DNA breaks to indirectly track the effect of the payload in cells over time. A pulse-chase approach was used to minimize confounding effects from the SN-38 payload released in media and subsequently entering cells. In this procedure, cells were incubated for an 8 hour 'pulse' with the three ADCs (structures in **Fig. 3A**), then replaced with complete media for a 24-, 48-, or 72-hour 'chase' phase (**Fig. 3B**). The rapid internalization of SG results in significant uptake during the pulse phase

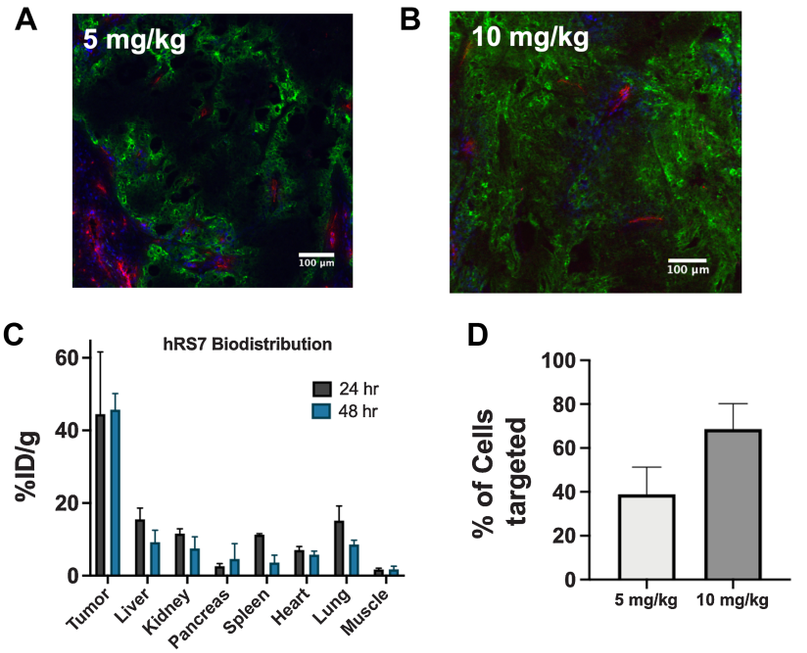

Figure 2.
Organ, tissue, and cellular biodistribution. Tissue penetration of hRS7 is dose-dependent, with a 5-mg/kg dose showing heterogeneous distribution after 24 hours (**A**), while the clinical dose of 10 mg/kg penetrates deeper into the tumor (**B**). Blood vessels are imaged with anti-CD31 stain (red), intravenous Hoechst 33342 is shown in blue, and hRS7-AlexaFluor680 is in green. The high expression and rapid internalization results in efficient tumor uptake ($n = 3$; **C**). Flow cytometry of single-cell suspensions at 24 hours from three different tumors at each dose confirms a greater proportion of cells are hRS7-AlexaFluor680 positive at the higher dose (**D**). Data are shown as the mean and SD.

(Supplementary Fig. S2). SG showed maximum γH2AX signal at 24 hours, indicating rapid payload release, which decreased over time. The nonspecific negative control ADC (h679-CL2A-SN-38) also showed maximum signal at 24 hours, though significantly lower than SG ($P < 0.05$). This indicates that some extracellular release occurred, though direct cell binding and internalization contributes to a greater portion of the PD signal. Finally, the ADC with enzyme cleavable linker (hRS7-CL2E-SN-38) only shows signal above the nonspecific negative control ADC at 72 hours, indicating slower release of the enzyme cleavable linker. This pattern was corroborated by confocal imaging of cells treated with the three ADCs (**Fig. 3C–E**), where SG shows elevated signal at 24 hours, followed by the nonbinding ADC, then the enzyme cleavable ADC.

SG exhibits more homogeneous and higher intensity PD staining *in vivo*

The payload distribution was next mapped *in vivo* using clinical ADC doses to establish the intensity of DNA damage and if the bystander effect was visible. Images confirm that the SN-38 payload diffuses to cells more distal to blood vessels, where the ADC backbone is not detectable (consistent with a bystander effect). SG shows relatively homogeneous payload distribution at 48 hours (**Fig. 4A**),

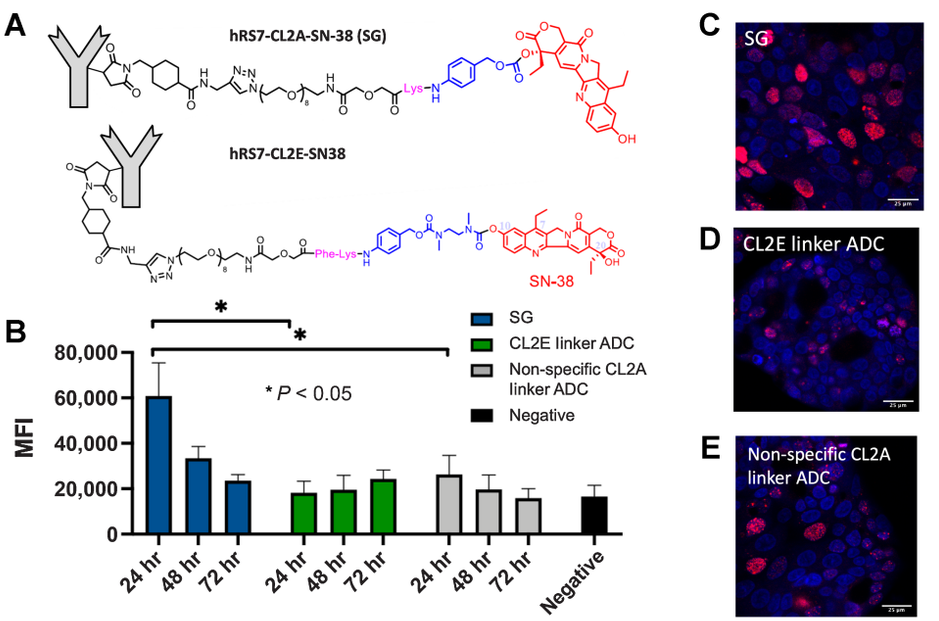

Figure 3.
In vitro Payload delivery and DNA damage. NCI-N87 cells were pulsed for 8 hours with SG (CL2A linker), the enzyme-cleavable (CL2E) linker ADC (structures shown in **A**), hydrolyzable (CL2A) linker nonspecific ADC, or left untreated and stained for DNA damage using γH2AX (**B**). Data show the median fluorescence intensity (MFI) and SD of three or four separate experiments. SG showed rapid and significant DNA damage that decreased over time, whereas the enzyme-cleavable CL2E linker ADC released the payload more slowly for lower signal that increased over 3 days. The hydrolyzable CL2A linker nonspecific control ADC showed some signal at 24 hours but lower than SG, highlighting the need for Trop-2–mediated targeting. Microscopy of NCI-N87 cells at the 24-hour time point showing nuclei (blue, Hoechst 33342) of cells treated with SG (**C**) with higher γH2AX signal (red) than the CL2E ADC (**D**) and nonspecific ADC (**E**).

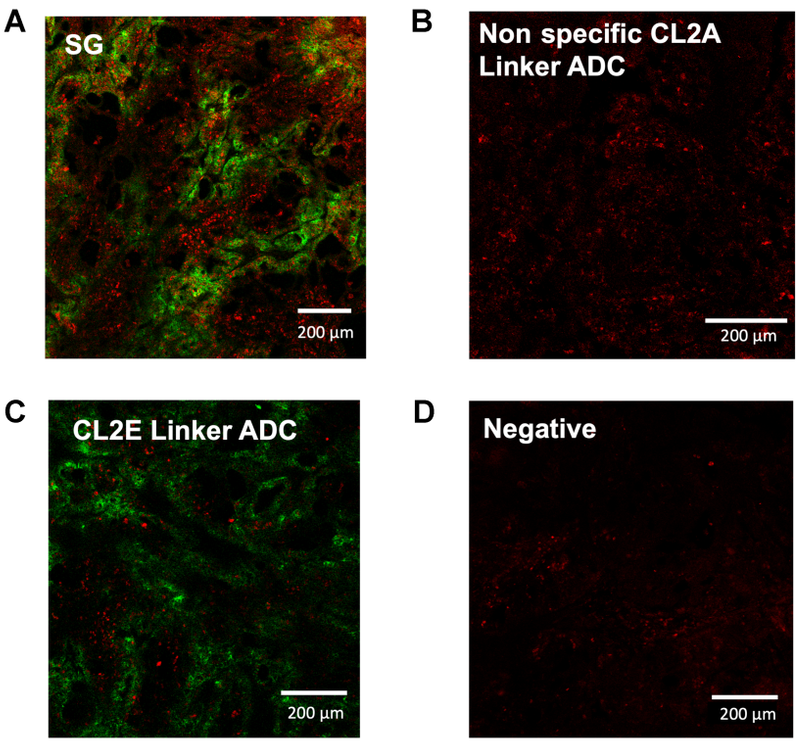

Figure 4.
In vivo imaging of ADC distribution and payload-mediated DNA damage. Forty-eight hours following a 10-mg/kg dose of SG (**A**), nonspecific CL2A-SN38 ADC (**B**), hRS7-CL2E-SN38 (**C**), or uninjected mice bearing NCI-N87 xenografts, tissue was excised and imaged using an anti-Fc stain (green) or γH2AX DNA damage marker (red). SG shows the highest signal including cells lacking ADC targeting (bystander effects). Signal from the other ADCs was lower but above background.

indicating that the bystander effect aids in delivering payload to untargeted (e.g., antigen-negative) cells. Interestingly, the nonspecific ADC control showed some PD signal despite no visible signal from the antibody itself via anti-Fc stain (**Fig. 4B**). This is consistent with *in vitro* PD staining where the nonbinding ADC causes some DNA damage, though at a lower intensity than SG. Some PD signal is detected after a 10-mg/kg dose of enzyme cleavable ADC (**Fig. 4C**), though it appears weaker and less widespread than SG, but higher than the nonspecific ADC, matching *in vitro* findings. These results are consistent with faster/more efficient payload release with a hydrolysable linker.

Dual-labeled technique determines location of payload release

While the PD signal patterns are consistent with the hypothesis that ADC efficacy is linked to more efficient payload release intracellularly, this does not exclude the hypothesis that extracellular payload release and bystander killing contribute to ADC efficacy. To examine this hypothesis, we employed a dual-labeled technique to determine the location of linker release. Both AF488 and AF680 behave as residualizing dyes (Supplementary Fig. S2), so they are trapped in cells after release (25). This property results from their charge and inability to cross plasma membranes. Therefore, they cannot diffuse into cells, and instead, they wash out of the tumor if released outside of cells (similar to nonbinding molecular imaging agents; ref. 26). Thus, we conjugated AF488 directly to the hRS7 antibody via a stable amide linkage that will only release the dye upon degradation of the antibody backbone after internalization. In addition, AF680 was conjugated to SN-38, which was attached to the hRS7 antibody via the CL2A linker. Because both dyes are expected to remain in cells if released intracellularly but cannot enter cells if released extracellularly, the ratio of AF680 to AF488 can be used to determine the location of payload release (**Fig. 5A**). Plasma clearance of the dual-labeled antibody was similar to unlabeled hRS7 antibody (Supplementary Fig. S3).

After a 10-mg/kg dose of dual-labeled hRS7 antibody, organ-level uptake was measured (%ID/g, **Fig. 5B**) and single-cell flow cytometry following tumor digestion shows the ratio of AF680 to AF488 in each cell (**Fig. 5C**). These values were normalized to untreated tumor cells labeled *ex vivo* with fully intact dual-labeled hRS7 antibody. At 24 hours, the ratio of AF680/AF488 remained the same as the *ex vivo* label, indicating no detectable extracellular release of SN38-AF680 occurred. At 48 hours, there was a 25% drop in the ratio of AF680/AF488, which could suggest that the CL2A linker bearing AF680 was cleaved outside of cells. However, this could occur systemically (e.g., in circulation) or in the tumor microenvironment. We examined the ratio of dyes in the plasma to distinguish between linker cleavage in the blood and the tumor (**Fig. 5D**). Using the AUC of plasma clearance, because AUC is proportional to tumor uptake, the data showed the AUC_{AF680}/AUC_{AF488} was about 0.75 at 48 hours (Supplementary Fig. S4). Minimal tumor uptake was seen from systemically administered SN38-AF680 (Supplementary Fig. S5). Therefore, the drop in ratio of AF680/AF488 at 48 hours measured on flow cytometry is attributed to linker deconjugation in the systemic circulation (e.g., plasma) before extravasating into the tumor rather than in the extracellular tumor space.

High and frequent dosing contributes to improved tissue penetration of SG

We next examined how the higher dosing of SG, 10 mg/kg on day 1 and day 8 of a 21-day cycle, impacted tumor uptake and tissue distribution. To study this, mice were injected with 10 mg/kg of unlabeled SG on day 1, followed by 5 mg/kg of fluorescent antibody on day 8, and organs were resected 24 hours later. 5 mg/kg was used for the second dose to ensure tumor uptake and distribution measurements were in a dynamic range because 10 mg/kg was close to tumor saturation, where changes in tissue penetration may not be distinguishable. Treatment with SG could impact tumor uptake of

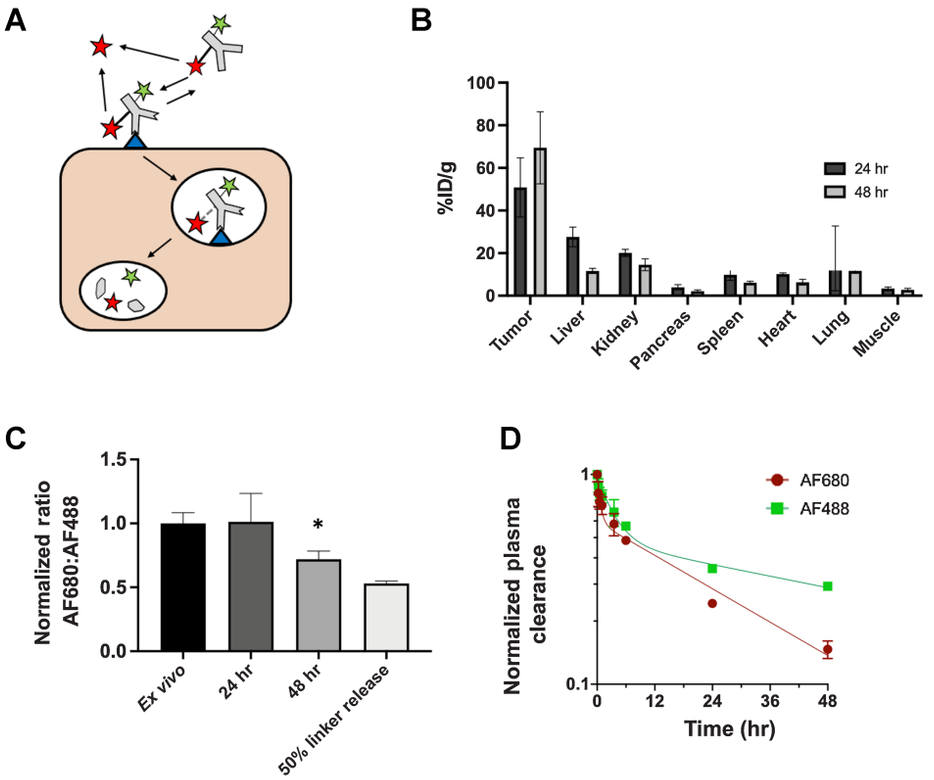

Figure 5.

Dual-labeled ADC for quantifying extracellular release. By labeling hRS7 antibody with two residualizing dyes, AF488 (green star) attached directly to antibody via a stable amide linkage and SN38-AF680 (red star) connected via the CL2A hydrolysable linker, the location of payload release could be quantified. Extracellular released SN38-AF680 dye (red star) is unable to enter cells and washes out of the tumor, while intracellularly released payload is trapped (**A**). Biodistribution (% injected dose/gram) of the dual-labeled ADC (as measured by SN38-AF680 signal) shows high tumor uptake, consistent with intracellular release and residualization of the dye (**B**). The ratio of AF680 to AF488 indicates little extracellular release of the payload in NCI-N87 tumors. There is a significant drop in the AF680 to AF488 ratio between the *ex vivo* control and the ratio at 48 hours ($P < 0.05$; **C**). The decreased ratio at 48 hours is less than the positive control cells labeled with ADC following 50% SN38-AF680 release. This lower ratio can be attributed to the loss of SN38-AF680 in systemic circulation, where AF680 signal decreases faster than AF488 in the plasma due to deconjugation (**D**). Data are shown as the mean and SD for $n = 3$ mice at each timepoint. An outlying point at 24 hours in the lung (15.9, 16.5, and 73%ID/g), likely from blood clotting during processing, resulted in a large standard deviation at 24 hours.

subsequent doses via multiple mechanisms, such as reduced delivery of a second dose following vascular collapse or increased perfusion and uptake following tumor cell death. However, biodistribution data showed identical uptake (%ID/g) of fluorescent antibody in the tumor on day 8 (**Fig. 6A**), which confirms that the initial dose does not change the uptake of the second dose. Interestingly, fluorescent histology images (tissue-level distribution; **Fig. 6B** and **C**) showed more homogeneous distribution of the second dose of fluorescent antibody compared with the same fluorescent antibody dose alone. This was confirmed by quantitative image analysis that mapped the fluorescent signal versus distance from blood vessels (**Fig. 6D**) by showing higher fluorescent signal farther from blood vessels. Therefore, treatment did not change the total amount of SG delivered but potentially improves tissue penetration.

Discussion

ADCs have experienced a surge in FDA approvals over the past few years, but the interplay of linker stability, payload potency and properties, target selection, and dosing has made design challenging. Here, we show an important mechanism driving the efficacy of SG is the high tissue penetration and rapid linker release inside cells. Although the design of SG is counterintuitive at first glance, these data clarify the efficacy advantage of a lower stability linker. We proposed two hypotheses that could explain the benefits of using a less stable linker: (i) extracellular linker cleavage in the tumor interstitium that better leverages the bystander effect (**Fig. 1B**) and/or (ii) more rapid payload release inside cells for more efficient cell killing (**Fig. 1C**), two mechanisms that are not mutually exclusive. Multiscale imaging and analysis of SG disposition were used to test these hypotheses and detail other delivery rates relevant to its positive therapeutic window.

ADC dosing is often limited by the toxicity of the conjugated payload, which prevents the use of saturating doses when the target antigen is highly expressed and/or rapidly internalized in the tissue (27). However, the use of SN-38, a moderately potent topoisomerase I inhibitor with a single-digit nanomolar IC_{50} (8), allows for higher dosing. In fact, SG has the highest dosing regimen of any clinically approved ADC (28). Challenges in overcoming the binding site barrier have been documented for Kadcyla, which treats $HER2^+$ breast cancer (29, 30). These studies also showed the connection between improved tissue penetration and efficacy (31). In this system,

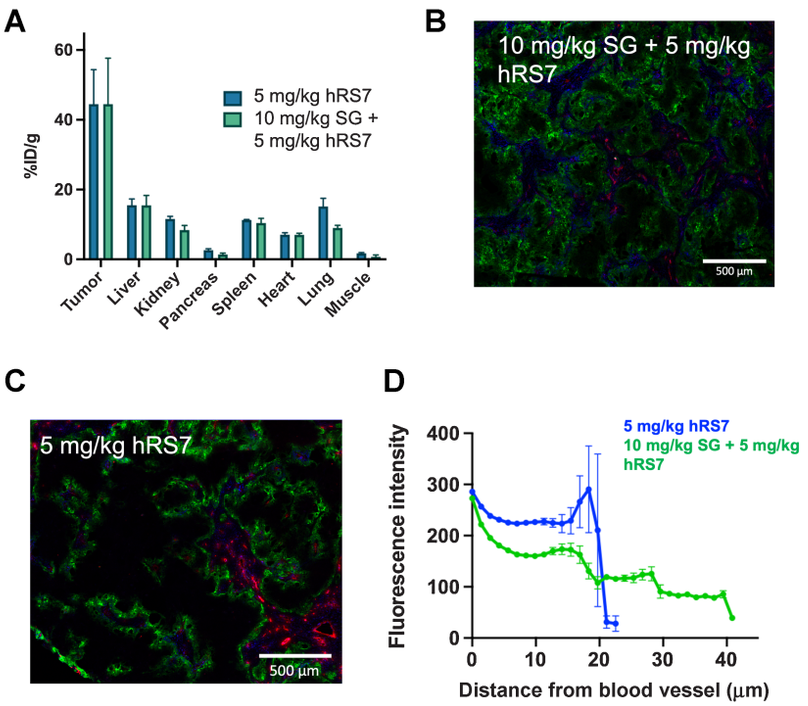

Figure 6.
Impact of Dosing Schedule. SG is dosed on D1 and D8 of a 21-day cycle. To examine the impact on distribution and uptake, 10 mg/kg SG was administered to mice bearing NCI-N87 xenografts, followed 7 days later by 5 mg/kg of fluorescent hRS7. The total tumor uptake (fluorescent %ID/g) was similar following SG treatment (mean and SD, $n = 3$; **A**). However, the distribution within the tumor was greater following SG treatment (**B**) than fluorescent hRS7 alone (**C**). CD31, red; intravenous Hoechst, blue; hRS7-AF680, green. Image quantification showing the mean and SEM using a Euclidean distance map confirmed deeper tissue penetration (**D**), which could be due to antibody from the SG treatment contributing to increased tissue penetration.

we established that a single clinical dose (10 mg/kg) reaches the majority of tumor cells (**Fig. 2**), which is an advantage of a moderately potent cytotoxic payload. This is particularly relevant for the rapidly internalized and highly expressed Trop-2 target, where a large dose is needed to achieve sufficient tissue penetration; in fact, even 10 mg/kg was not fully saturating in mice. However, the maximum concentrations achieved in humans are approximately 1.9× higher than those in mice, potentially allowing full saturation in the clinic. It was also unclear how two doses in each cycle would influence tumor uptake and distribution, and if the collapse of blood vessels or formation of new vessels could improve or hinder tumor targeting of second doses. Interestingly, the tumor uptake of the second dose was the same as the first dose (**Fig. 6A**), though histology imaging showed more homogeneous distribution of the second dose (**Fig. 6C** and **D**). The first 10-mg/kg dose is still circulating after 1 week based on measured pharmacokinetics from the blood (Supplementary Fig. S6A). While most of the payload would be deconjugated after a week, the remaining antibody can compete for binding sites with the second dose (similar to an antibody 'carrier dose'), allowing it to penetrate further into the tissue. This mechanism was corroborated with Krogh cylinder simulations (Supplementary Fig. S6B), although alternatives, such as faster diffusion following cell death/reduced packing density, could not be ruled out. These findings are also likely to apply clinically, as heterogeneous antibody distribution has been documented in clinical tumors, and have shown improvement with an antibody 'carrier dose' (effectively increasing the antibody dose; ref. 32).

The counterintuitive benefit in efficacy from a lower stability linker became apparent when investigating the appearance of PD signal in cells after brief incubations with three different ADCs (**Fig. 3**). Though some of the SG PD signal at 24 hours can be attributed to payload released extracellularly in the media, the nonspecific control ADC shows less DNA damage, and both show significantly more signal from the ADC with the hydrolyzable linker (CL2A) than the enzyme-cleavable linker (CL2E). This is also translated *in vivo*, where enzyme cleavable ADCs were not as effective as ADCs with the CL2A linker (14, 15). The CL2E linker is likely cleaved effectively by lysosomal enzymes (33), but the data indicate more rapid release of the CL2A linker accounts for the differences in efficacy between the two linkers (where the CL2E linker never achieves high signal, even at later time, Supplementary Fig. S7). This emphasizes the importance of efficient intracellular payload release, which has been supported by other studies. For example, Devay and colleagues showed the importance of efficient lysosomal trafficking with a Trop-2 bispecific antibody where the second arm binds a target that is directed efficiently to the lysosome (17). In this case, more efficient lysosomal trafficking resulted in greater efficacy, likely due to more efficient payload release. Furthermore, other studies have demonstrated that delays in payload trafficking decrease cell killing ability and could be mechanisms of resistance (34, 35).

The improved efficacy of the CL2A versus CL2E linker demonstrated by previous studies was corroborated by PD imaging of tumors that showed the strongest PD staining for SG. This data also confirmed that the bystander effect is visible in tumors, with PD staining beyond the region targeted by these ADCs (**Fig. 4**). Although the multiscale distribution studies confirmed that most cells were targeted by the high antibody dosing, bystander effects are likely an important mechanism given the documented intratumoral heterogeneity in surface marker expression (36, 37). Bystander killing can offset heterogeneity in antibody distribution (spatial bystander effect) or antigen-negative cells (heterogeneous bystander effect) to reach a greater number of cancer cells than non-bystander payloads (38). Others have explored the possibility of non-internalizing ADCs, where the ADC accumulates in the tumor by binding to cells and releases the payload outside of cells (39–41). This further raises the potential for extracellular payload release, which could allow for greater efficiency of the bystander effect by reducing the number of steps the payload needs to undergo to reach an untargeted cell (**Fig. 1B**).

The extracellular release mechanism could occur in addition to more efficient intracellular release. Although the rapid internalization relative to linker cleavage would suggest most payload is delivered inside cancer cells before release in the tumor, the hydrolysable nature of the linker at the pH of the tumor microenvironment could result in payload released extracellularly *in vivo*. In fact, we observed some PD signal when using a nonbinding control ADC (**Fig. 4C**), likely from some accumulation in the tumor due to the enhanced permeability and retention effect (42). Preclinical studies with nonbinding ADCs conjugated to SN-38 via the CL2A linker showed slight efficacy, though less than specific ADCs (8). This indicates extracellular release of the CL2A linker can occur. Therefore, we sought to measure extracellular payload release *in vivo*.

To quantify the extracellular drug release, a dual-labeled fluorescence method (**Fig. 5A**) was used, and the results indicated that extracellular release was not significant in this model. Because both dyes remain trapped in cells after release, a lower ratio of AF680/AF488 (where AF680 is conjugated to SN-38 of CL2A-SN38) would indicate some extracellular release in the tumor. While we observed a decrease in this ratio on flow cytometry at 48 hours compared with an *ex vivo* control labeled with fully intact dual-labeled antibody, this can be attributed to linker cleavage in systemic circulation as determined by the ratio in AUC from plasma clearance data (**Fig. 5D**), which is proportional to tumor uptake. Given the relatively fast internalization rate of Trop-2 ($t_{1/2} = 4.16$ hours, Supplementary Fig. S2), the extracellular drug release from receptor-bound SG ($t_{1/2} = 21$ hours; ref. 14) is likely negligible compared with the amount of SN-38 delivered directly through receptor-mediated internalization. One limitation of the current approach is that the conjugation of AF680 to SN-38 slowed down the rate of linker hydrolysis approximately 3-fold ($t_{1/2} =$ 58.7 hours, Supplementary Fig. S8), which makes the method less sensitive to small amounts of payload released. However, both rates of release are slower than Trop-2 internalization, consistent with little extracellular release for the targeted ADCs in a Trop-2 model.

In addition to the less stable linker helping overall efficacy, it also appears to reduce target-mediated toxicity. Most ADCs are engineered for a highly stable linker in circulation to avoid (off-target) systemic toxicity (12). The CL2A linker stability has a half-life of about a day in circulation (14), but maintains its efficacy and tolerability. Trop-2 has low but significant expression in some healthy tissues (43), which can lead to on-target, off-tumor toxicity. SG likely avoids this on-target toxicity (e.g., stomatitis) because some payload is shed from the ADC before substantial accumulation in healthy tissues, so less payload is delivered compared with other Trop-2 targeted ADCs with more stable linkers (16, 44). In addition, because SN-38 is only moderately potent, free payload shed in circulation is better tolerated than ultra-potent payloads.

While this work establishes how using a less stable linker with a moderately potent payload at high doses is effective for SG, that does not mean lower stability linkers are optimal in all circumstances. Like all aspects of ADCs, the properties need to be tailored to the specific target. For example, in lower expression systems, the higher dosing may be supersaturating, and a moderately potent payload may not be potent enough to kill targeted cells. Previous work has emphasized that matching the potency of the payload to cellular delivery can optimize ADC efficacy (30).

Because SN-38 is approved in other formulations, such as irinotecan and a liposomal formulation (Onivyde), a conceptual question is whether SG is behaving as a nonspecific drug carrier or a typical ADC (45). The rapid internalization seen here indicates that most ADC uptake in the tumor results in intracellular payload delivery for high Trop-2 expression tumors. Therefore, the relevant comparison for this distinction is between sustained systemic release of SN-38 versus the typical ADC cellular internalization and release mechanism. Sharkey and colleagues showed a 10-fold higher cumulative SN-38 uptake in tumor versus serum for SG compared with more serum SN-38 than tumor uptake for irinotecan, indicating better tumor delivery for SG (46). They also showed between 20- and 50-fold higher AUC for SN-38 delivered to tumors with SG compared with irinotecan, supporting the typical ADC intratumoral delivery as the conceptual mechanism. The current data indicate the lack of efficacy for CL2E is not due to a lack of sustained systemic release but rather inefficient release inside cells. *In vivo* data indicate that SG efficacy is related to target expression, because nonspecific ADCs with the CL2A linker or SG with antigen-negative tumors have poor responses (47). Likewise, clinical data for TNBC shows higher response rates and more durable progression-free survival with higher Trop-2 expression (48, 49). This is consistent with Trop-2 mediated targeting increasing the efficacy of SN-38. Other nonspecific carriers of SN-38 have shown shorter periods of progression-free survival than SG in TNBC, e.g., 4.3 months versus 6 months (10, 50). However, this does not preclude systemically released payload or non-internalized ADC in antigen-negative tumors from contributing to efficacy; this likely plays a role in efficacy for patients with low Trop-2 expression. Rather, sustained systemic release of SN-38 versus ADC-driven targeting is a quantitative distinction, and Trop-2–mediated delivery appears to play a significant role in response rates for many patients. Therefore, these data support the importance of Trop-2–mediated delivery even if systemic payload release adds to these effects in some cases.

In conclusion, these results clarify the mechanism of action for SG. The moderately potent payload allows high ADC dosing to improve tissue penetration, and rapid internalization and payload release from the hydrolysable CL2A linker efficiently delivers the payload intracellularly, which increases efficacy compared with a more stable protease-cleavable linker (CL2E). The SN-38 payload can still exhibit bystander effects following intracellular release to target antigen-negative cells. A second dose after 1 week has similar tumor uptake but may improve tissue penetration from residual antibody in circulation. Finally, the systemic payload release appears to reduce target-mediated off-tumor toxicity, and the moderate potency payload maintains tolerability. Together, this type of holistic, quantitative approach can aid in ADC design for a given target, payload type/potency, and linker type to improve treatment efficacy.

Authors' Disclosures

S. Hofsess reports other support from Gilead Sciences, Inc. outside the submitted work. T.M. Cardillo reports other support from Gilead Sciences outside the submitted work. S.V. Govindan reports other support from Immunomedics, Inc.; and other support from Gilead Sciences, Inc. during the conduct of the study; in addition, S.V. Govindan has a patent for US patent 7,999, 083 B2 and related US patents and international patents issued. G.M. Thurber reports grants and nonfinancial support from Immunomedics; and grants from NIH during the conduct of the study; personal fees from AstraZeneca/Medimmune, Advanced Proteome Therapeutics, Catalent, Mersana, Neoleukin, Gilead, Seattle Genetics, Roche/Genentech, AbbVie, Bristol-Myers Squibb; grants from Takeda Pharmaceuticals, Crescendo Biologics; other support from CytomX Therapeutics, Novartis; nonfinancial support from Immunogen, Synaffix; and grants from Iksuda outside the submitted work. No disclosures were reported by the other authors.

Authors' Contributions

A. Kopp: Conceptualization, formal analysis, investigation, visualization, methodology, writing–original draft, writing–review and editing. **S. Hofsess:** Conceptualization, resources, data curation, funding acquisition, writing–original draft, project

administration, writing–review and editing. **T.M. Cardillo:** Conceptualization, resources, data curation, supervision, visualization, writing–original draft, writing–review and editing. **S.V. Govindan:** Conceptualization, resources, data curation, investigation, methodology, writing–original draft, writing–review and editing. **J. Donnell:** Resources, investigation, methodology. **G.M. Thurber:** Conceptualization, formal analysis, supervision, funding acquisition, writing–original draft, project administration, writing–review and editing.

Acknowledgments

Support for this work was provided by Gilead Sciences, Inc., NIH Grant R35 (GM128819), and P30 CA046592. This material is based upon work supported by the National Science Foundation Graduate Research Fellowship Program under Grant No. 1841052 (to A. Kopp).

We acknowledge David M. Goldenberg, ScD, MD (Founder and former Chairman and CSO of *Immunomedics*, acquired by *Gilead Sciences*) for directing the preclinical and the clinical development of ADCs including Trop-2–targeted SG, and Robert M. Sharkey, PhD (Former Sr. Director of Scientific and Regulatory Affairs, *Immunomedics*) for contributions to elucidating the properties of SG and to the initial clinical studies.

The publication costs of this article were defrayed in part by the payment of publication fees. Therefore, and solely to indicate this fact, this article is hereby marked "advertisement" in accordance with 18 USC section 1734.

Note

Supplementary data for this article are available at Molecular Cancer Therapeutics Online (http://mct.aacrjournals.org/).

Received May 27, 2022; revised August 5, 2022; accepted September 27, 2022; published first October 3, 2022.

References

1. Goldenberg DM, Stein R, Sharkey RM. The emergence of trophoblast cell-surface antigen 2 (Trop-2) as a novel cancer target. Oncotarget 2018;9: 28989–9006.
2. Ambrogi F, Fornili M, Boracchi P, Trerotola M, Relli V, Simeone P, et al. Trop-2 is a determinant of breast cancer survival. PLoS One 2014;9:96993.
3. Zeng P, Chen MB, Zhou LN, Tang M, Liu CY, Lu PH. Impact of Trop-2 expression on prognosis in solid tumors: a systematic review and meta-analysis. Sci Rep 2016;6:33658.
4. Pommier Y. Topoisomerase I inhibitors: camptothecins and beyond. Nat Rev Cancer 2006;6:789–802.
5. Vasalou C, Helmlinger G, Gomes B. A mechanistic tumor penetration model to guide antibody–drug conjugate design. PLoS One 2015;10:e0118977.
6. Beck A, Goetsch L, Dumontet C, Corvaïa N. Strategies and challenges for the next generation of antibody–drug conjugates. Nat Rev Drug Discov 2017;16: 315–37.
7. Cardillo TM, Govindan SV, Sharkey RM, Trisal P, Arrojo R, Liu D, et al. Sacituzumab govitecan (IMMU-132), an anti–Trop-2/SN-38 antibody–drug conjugate: characterization and efficacy in pancreatic, gastric, and other cancers. Bioconjug Chem. 2015;26:919–31.
8. Cardillo TM, Govindan SV, Sharkey RM, Trisal P, Goldenberg DM. Humanized anti–Trop-2 IgG-SN-38 conjugate for effective treatment of diverse epithelial cancers: preclinical studies in human cancer xenograft models and monkeys. Clin Cancer Res 2011;17:3157–69.
9. Starodub AN, Ocean AJ, Shah MA, Guarino MJ, Picozzi VJ, Vahdat LT, et al. First-in-human trial of a novel anti–Trop-2 antibody-SN-38 conjugate, sacituzumab govitecan, for the treatment of diverse metastatic solid tumors. Clin Cancer Res 2015;21:3870–8.
10. Bardia A, Mayer IA, Diamond JR, Moroose RL, Isakoff SJ, Starodub AN, et al. Efficacy and safety of anti–trop-2 antibody–drug conjugate sacituzumab govitecan (IMMU-132) in heavily pretreated patients with metastatic triple-negative breast cancer. J Clin Oncol 2017;35:2141–8.
11. Faltas B, Goldenberg DM, Ocean AJ, Govindan SV, Wilhelm F, Sharkey RM, et al. Sacituzumab govitecan, a novel antibody–drug conjugate, in patients with metastatic platinum-resistant urothelial carcinoma. Clin Genitourin Cancer 2016;14:e75–9.
12. Donaghy H. Effects of antibody, drug, and linker on the preclinical and clinical toxicities of antibody–drug conjugates. MAbs 2016;8:659–71.
13. Panowski S, Bhakta S, Raab H, Polakis P, Junutula JR. Site-specific antibody–drug conjugates for cancer therapy. MAbs 2014;6:34–45.
14. Govindan SV, Cardillo TM, Sharkey RM, Tat F, Gold DV, Goldenberg DM. Milatuzumab-SN-38 conjugates for the treatment of CD74$^+$ cancers. Mol Cancer Ther 2013;12:968–78.
15. Govindan SV, Cardillo TM, Rossi EA, Trisal P, McBride WJ, Sharkey RM, et al. Improving the therapeutic index in cancer therapy by using antibody–drug conjugates designed with a moderately cytotoxic drug. Mol Pharm 2015;12: 1836–47.
16. Strop P, Tran T-T, Dorywalska M, Delaria K, Dushin R, Wong OK, et al. RN927C, a Site-specific Trop-2 antibody–drug conjugate (ADC) with enhanced stability, is highly efficacious in preclinical solid tumor models. Mol Cancer Ther 2016;15:2698–708.
17. DeVay RM, Delaria K, Zhu G, Holz C, Foletti D, Sutton J, et al. Improved lysosomal trafficking can modulate the potency of antibody–drug conjugates. Bioconjug Chem 2017;28:1102–14.
18. Singh AP, Sharma S, Shah DK. Quantitative characterization of *in vitro* bystander effect of antibody–drug conjugates. J Pharm Sci 2016;43:567–82.
19. Perrone E, Manara P, Lopez S, Bellone S, Bonazzoli E, Manzano A, et al. Sacituzumab govitecan, an antibody–drug conjugate targeting trophoblast cell-surface antigen 2, shows cytotoxic activity against poorly differentiated endometrial adenocarcinomas *in vitro* and *in vivo*. Mol Oncol 2020;14: 645–56.
20. Khera E, Dong S, Huang H, de Bever L, van Delft FL, Thurber GM. Cellular-resolution imaging of bystander payload tissue penetration from antibody–drug conjugates. Mol Cancer Ther 2021;15:310–21.
21. Khera E, Cilliers C, Bhatnagar S, Thurber GM. Computational transport analysis of antibody–drug conjugate bystander effects and payload tumoral distribution: implications for therapy. Mol Syst Des Eng 2018;3:73–88.
22. Sharkey RM, Govindan SV, Cardillo TM, Goldenberg DM. Epratuzumab-SN-38: a new antibody–drug conjugate for the therapy of hematologic malignancies. Mol Cancer Ther 2012;11:224–34.
23. Cilliers C, Nessler I, Christodolu N, Thurber GM. Tracking antibody distribution with near-infrared fluorescent dyes: impact of dye structure and degree of labeling on plasma clearance. Mol Pharm. 2017;14:1623–33.
24. Cilliers C, Guo H, Liao J, Christodolu N, Thurber GM. Multiscale modeling of antibody–drug conjugates: connecting tissue and cellular distribution to whole animal pharmacokinetics and potential implications for efficacy. AAPS J 2016; 18:1117–30.
25. Cilliers C, Liao J, Atangcho L, Thurber GM. Residualization rates of near-infrared dyes for the rational design of molecular imaging agents. Mol Imaging Biol 2015;17:757–62.
26. Bhatnagar S, Verma KD, Hu Y, Khera E, Priluck A, Smith DE, et al. Oral administration and detection of a Near-infrared molecular imaging agent in an orthotopic mouse model for breast cancer screening. Mol Pharm 2018;15: 1746–54.
27. Thurber GM, Zajic SC, Wittrup KD. Theoretic criteria for antibody penetration into solid tumors and micrometastases. J Nucl Med 2007;48:995–9.
28. Nessler I, Menezes B, Thurber GM. Key metrics to expanding the pipeline of successful antibody–drug conjugates. Trends Pharmacol Sci 2021;42:803–12.
29. Bordeau BM, Yang Y, Balthasar JP. Transient competitive inhibition bypasses the binding site barrier to improve tumor penetration of trastuzumab and enhance T-DM1 efficacy. Cancer Res 2021;81:4145–54.
30. Cilliers C, Menezes B, Nessler I, Linderman J, Thurber GM. Improved tumor penetration and single-cell targeting of antibody–drug conjugates increases anticancer efficacy and host survival. Cancer Res 2018;78:758–68.
31. Nessler I, Khera E, Vance S, Kopp A, Qiu Q, Keating TA, et al. Increased tumor penetration of Single-domain antibody–drug conjugates improves *in vivo* efficacy in prostate cancer models. Cancer Res 2020;80:1268–78.
32. Lu G, Nishio N, van den Berg NS, Martin BA, Fakurnejad S, van Keulen S, et al. Co-administered antibody improves penetration of antibody–dye conjugate into human cancers with implications for antibody–drug conjugates. Nat Commun 2020;11:1–11.

33. Caculitan N±AG, dela Cruz Chuh J, Ma Y, Zhang D, Kozak KR, Liu Y, et al. Cathepsin B is dispensable for cellular processing of cathepsin B-cleavable Antibody–drug conjugates. Cancer Res 2017;77:7027–37.
34. Tsui CK, Barfield RM, Fischer CR, Morgens DW, Li A, Smith BAH, et al. CRISPR-Cas9 screens identify regulators of antibody–drug conjugate toxicity. Nat Chem Biol 2019;15:949–58.
35. Hamblett KJ, Jacob AP, Gurgel JL, Tometsko ME, Rock BM, Patel SK, et al. SLC46A3 is required to transport catabolites of noncleavable antibody maytansine conjugates from the lysosome to the cytoplasm. Cancer Res 2015;75:5329–40.
36. Singh AP, Seigel GM, Guo L, Verma A, Wong GG-L, Cheng H-P, et al. Evolution of the systems pharmacokinetics-pharmacodynamics model for antibody–drug conjugates to characterize tumor heterogeneity and *in vivo* bystander effect. J Pharmacol Exp Ther 2020;374:184–99.
37. Seol H, Lee HJ, Choi Y, Lee HE, Kim YJ, Kim JH, et al. Intratumoral heterogeneity of HER2 gene amplification in breast cancer: its clinicopathological significance. Mod Pathol 2012;25:938–48.
38. Burton JK, Bottino D, Secomb TW. A Systems Pharmacology model for drug delivery to solid tumors by antibody–drug conjugates: Implications for bystander effects. AAPS J 2020;22:12.
39. Dal Corso A, Gébleux R, Murer P, Soltermann A, Neri D. A non-internalizing antibody–drug conjugate based on an anthracycline payload displays potent therapeutic activity *in vivo*. J Control Release 2017;264:211–8.
40. Gébleux R, Stringhini M, Casanova R, Soltermann A, Neri D. Non-internalizing antibody–drug conjugates display potent anti-cancer activity upon proteolytic release of monomethyl auristatin E in the subendothelial extracellular matrix. Int J Cancer 2017;140:1670–9.
41. Dal Corso A, Cazzamalli S, GÃ©bleux R©M, Mattarella M, Neri D. Protease-cleavable linkers modulate the anticancer activity of non-internalizing antibody—drug conjugates. Bioconjug Chem 2017;28:1826–33.
42. Iyer AK, Khaled G, Fang J, Maeda H. Exploiting the enhanced permeability and retention effect for tumor targeting. Drug Discov Today 2006;11:812–8.
43. Trerotola M, Cantanelli P, Guerra E, Tripaldi R, Aloisi AL, Bonasera V, et al. Upregulation of Trop-2 quantitatively stimulates human cancer growth. Oncogene 2013;32:222–33.
44. Okajima D, Yasuda S, Maejima T, Karibe T, Sakurai K, Aida T, et al. Datopotamab deruxtecan, a novel Trop-2–directed antibody–drug conjugate, demonstrates potent antitumor activity by efficient drug delivery to tumor cells. Mol Cancer Ther 2021;20:2329–40.
45. Santi DV, Cabel L, Bidard F-C. Does sacituzumab-govitecan act as a conventional antibody–drug conjugate (ADC), a prodrug of SN-38 or both? Ann Transl Med 2021;9:1113.
46. Sharkey RM, McBride WJ, Cardillo TM, Govindan SV, Wang Y, Rossi EA, et al. Enhanced delivery of SN-38 to human tumor xenografts with an anti–Trop-2-SN-38 antibody conjugate (sacituzumab govitecan). Clin Cancer Res 2015;21:5131–8.
47. Goldenberg DM, Cardillo TM, Govindan SV, Rossi EA, Sharkey RM. Trop-2 is a novel target for solid cancer therapy with sacituzumab govitecan (IMMU-132), an antibody–drug conjugate (ADC). Oncotarget 2015;6:22496–512.
48. Gray JE, Heist RS, Starodub AN, Camidge DR, Kio EA, Masters GA, et al. Therapy of small cell lung cancer (SCLC) with a topoisomerase I–inhibiting antibody–drug conjugate (ADC) targeting Trop-2, sacituzumab govitecan. Clin Cancer Res 2017;23:5711–9.
49. Helwick C. Is Trop-2 expression associated with benefit from sacituzumab govitecan? The ASCO Post 2021. Available from: https://ascopost.com/issues/february-10-2021/is-trop-2-expression-associated-with-benefit-from-sacituzumab-govitecan/.
50. Sachdev JC, Munster P, Northfelt DW, Han HS, Ma C, Maxwell F, et al. Phase I study of liposomal irinotecan in patients with metastatic breast cancer: findings from the expansion phase. Breast Cancer Res Treat 2021;185:759–71.